Ultrasonics Sonochemistry 117 (2025) 107336

Contents lists available at ScienceDirect

Ultrasonics Sonochemistry

journal homepage: www.elsevier.com/locate/ultson

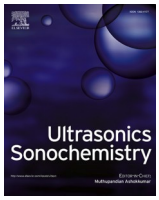

Short communication

Enhancing ultrasound applications through shell-less nanobubbles: A study on acoustic and optical properties

Zong-Han Hsieh [a], Cheng-An J. Lin [b], Chih-Kuang Yeh [a,*]

[a] Department of Biomedical Engineering and Environmental Sciences, National Tsing-Hua University, Hsinchu, Taiwan
[b] Department of Biomedical Engineering, Chung Yuan Christian University, Taoyuan, Taiwan

ARTICLE INFO

Keywords:
Nanobubble
Claw-type pump
Ultrasound
Inertial cavitation

ABSTRACT

Histotripsy employs acoustic inertial cavitation to mechanically destroy tissue, producing acellular debris. While introducing bubbles can lower the cavitation threshold and enhance treatment efficiency, micrometer-scale bubbles struggle to penetrate tissues effectively. Shell-less nanobubbles, with their high internal pressure, stability, negatively charged surfaces, and unique lifetimes ranging from weeks to months, offer a promising alternative. However, their interactions with ultrasound remain unexplored. This study used a claw-type pump nanobubble generator to produce nanobubbles and employed acoustic and optical methods to observe their behavior under high-intensity ultrasound exposure. The results demonstrated that the device generated nanobubble solutions with an average particle size of 107 nm, a concentration of 1.94×10^9 particles/mL, a lifetime exceeding one week, and a zeta potential of −21.2 mV. Acoustic and optical observations further revealed that nanobubble solutions reduced the inertial cavitation threshold of the liquid from 26.5 MPa to 10.3 MPa. These findings suggest a potential strategy to enhance the efficiency of ultrasound histotripsy treatments.

1. Introduction

In medical ultrasound, treatments such as histotripsy rely on the acoustic inertial cavitation effect to mechanically destroy tissue, rendering the target into acellular debris [1]. The cavitation threshold has been reported to be 26–30 MPa for water-based tissues [2]. Introducing bubbles is a potential method to lower the inertial cavitation threshold [3] and enhancing treatment efficiency. However, micrometer-scale bubbles are too large to penetrate tissues effectively.

Due to their smaller size compared to microbubbles, nanobubbles present a potential solution. In recent years, nanosized lipid-shell bubbles have been commonly used as contrast agents for enhancing ultrasound imaging [4,5] or drug delivery [6]. The interactions between these carriers and ultrasound have been extensively explored and discussed [7]. However, these lipid-shelled nanobubbles are not small enough, are challenging to manufacture, and are relatively expensive. As a result, shell-less nanobubbles may offer a promising alternative to address these limitations.

Current mainstream studies suggest that when shell-less bubbles shrink to the nanoscale, the bubbles no longer spontaneously rise to the surface of the liquid and burst. Instead, they undergo Brownian motion in place[8], and their internal pressure significantly increases, enhancing bubble stability and granting them a lifetime of several weeks to months [9]. Additionally, another study has reported that nanobubbles carry a negative surface charge and can be affected by gas composition, pH, temperatures, and salt concentrations[10], which can enhance the dissolved oxygen content in solutions [11,12] and reduce surface tension [13–17]. These theoretical mechanisms have led to applications of nanobubbles in fields such as water purification in aquaculture [18,19], water treatment [20], and accelerated agricultural growth [21]. However, there has been limited research on the interaction between shell-less nanobubbles and high-intensity ultrasound.

According to theoretical predictions, the diameter of such bubbles is far smaller than the wavelength of ultrasound, and their significant internal pressure makes them nearly impervious to vibration or collapse induced by ultrasound [20]. In this study, we aim to use acoustic and optical methods to observe the behavior of nanobubbles under the impact of high-intensity ultrasound, thereby elucidating their interactions. Ultimately, this research seeks to apply this type of nanobubbles in the ultrasound field.

* Corresponding author at: Department of Biomedical Engineering and Environmental Sciences, National Tsing Hua University, No. 101, Section 2, Kuang-Fu Road, Hsinchu 30013, Taiwan.
E-mail address: ckyeh@mx.nthu.edu.tw (C.-K. Yeh).

https://doi.org/10.1016/j.ultsonch.2025.107336
Received 23 January 2025; Received in revised form 19 March 2025; Accepted 28 March 2025
Available online 5 April 2025

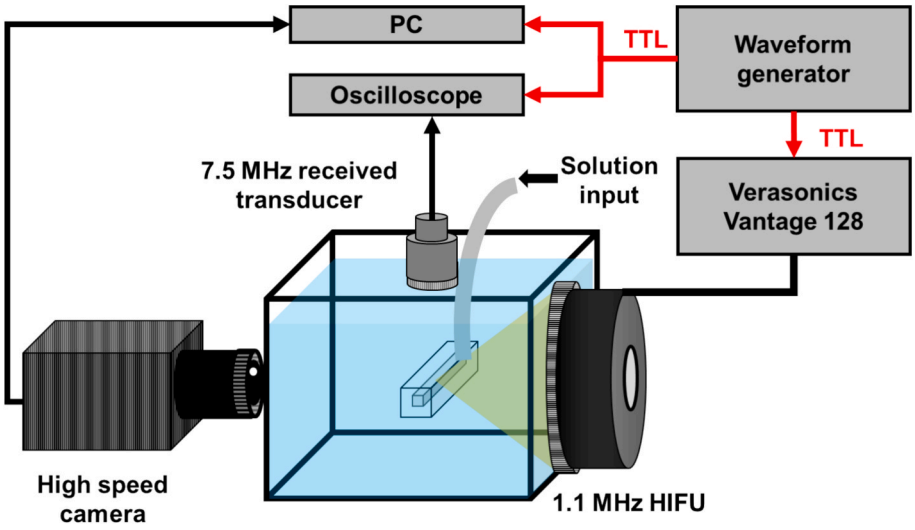

Fig. 1. The experimental setup to measure the acoustic feature of the nanobubbles.

To achieve this goal, the study first utilized a claw-type pump nanobubble generator, which employs two claw-shaped rotors mounted in a cylinder that move in opposite directions to produce nanobubbles in the flowing liquid. According to the literature, nanobubble generation methods can be categorized into the membrane, pressurized dissolution, Venturi effect, swirl liquid flow, breakup effect of high shear stress [22], and acoustic cavitation [23]. The mechanism of nanobubble generation by the claw-type pump method is similar to a combination of the swirl liquid flow and the breakup effect of high shear stress methods. Next, the fundamental properties of the nanobubbles, including size, concentration, lifetime, and zeta potential, were measured. Finally, high-speed optical imaging and an acoustic passive cavitation detection method were employed to verify their acoustic properties.

2. Methods

2.1. Basic properties of nanobubbles

In this study, a nanobubble generator (Model: P40D50T20S20U, LIUNG FENG INDUSTRIAL CO., LTD., New Taipei, Taiwan) was used to produce nanobubble solutions [24]. The device operates by circulating deionized (DD) water through the machine for 30 min, after which the nanobubble-containing solution is collected from the outlet. Light scattering was first utilized for observation to confirm the solution's properties. A 532 nm green laser (MGL-III-532-50mW, Changchun New Industries Optoelectronics Technology, Changchun, China) was directed at containers holding DD water and the nanobubble solutions. If nanoparticles smaller than the wavelength of light were present in the solution, the laser beam would scatter due to Rayleigh scattering, which can be directly observed. After confirming the presence of nanoparticles in the solution, this study referenced the literature and employed the freezing and thawing method to verify whether the particles in the solution were indeed gas bubbles [25]. This method involves freezing the bubbles in the solution and removing them during thawing. The experimental procedure involved freezing 15 mL of DD water and the nanobubble solution in a −20 °C freezer for 24 h, followed by thawing at room temperature (25 °C) for 6 h. The optical density (OD) before and after freezing and thawing was measured using a spectrophotometer (Infinite® 200PRO series, Tecan, AG, Switzerland) to indicate the existence of nanobubbles, as the scattering effect of the nanobubbles increases the OD value in the solution. After confirming the presence of nanobubbles in the solution, the OD values of DD water and the nanobubble solution were measured on days 0, 1, and 7 to assess their lifetime. Additionally, following ISO/TC281 standards, the concentration, size distribution, and zeta potential of nanobubbles were determined using a NanoSight (NS300, Malvern, UK) and dynamic light scattering (DLS) (Autosizer 4700; Malvern, Worcestershire, UK).

2.2. Acoustic properties of nanobubbles

According to previous studies, the intense internal pressure of nanobubbles makes it difficult for them to interact with low-energy ultrasound [20]. Therefore, this study aims to observe the characteristics of nanobubbles under high acoustic pressure using optical and acoustic methods. The experimental setup is shown in Fig. 1. An agar phantom with a 3.5 mm diameter tubular channel was fabricated and connected to a plastic tube to introduce DD water and nanobubbles (NB) solution. Additionally, a 2×10^8 particles/ml homemade microbubble (MB) contrast agent [26] was added as a positive control (The detail of the MB solution measurement can be seen in the support information). The 1.1 MHz HIFU transducer (H-301, Sonic Concepts, Bothell, WA, USA), high-speed camera (Photron SA1.1, U&U International Inc, Taipei, Taiwan), and 7.5 MHz receiving transducer (V321, Olympus, Tokyo, Japan) were aligned to the tubular channel inside the phantom to observe the behavior of samples during ultrasonic excitation. The 1.1 MHz HIFU transducer (aperture size = 15 cm, focal depth = 15 cm) was connected to a Verasonics system (Vantage128, Verasonics, Kirkland, WA, USA) and driven to emit ultrasound using a 5 to 60 V, 1.1 MHz, 100-cycle, single-pulse signal. The acoustic signal was measured with a hydrophone (HGL-0085, ONDA, Sunnyvale, CA, USA), revealing an acoustic pressure range of 2.6 to 32 MPa. The high-speed camera, connected to a computer, captured images at 10,000 fps with a shutter time of 19 μs to observe the changes in the sample when the ultrasound reached it. The 7.5 MHz receiving transducer (Bandwidth: 4.74–9.49 MHz) was connected to an oscilloscope for passively receiving signals. According to the literature, when high acoustic pressure ultrasound is applied, gas nuclei in the water will be excited into bubbles, generating a wideband signal that can be passively detected by the receiving transducer [27]. This phenomenon is known as the inertial cavitation effect, which can be quantified by integrating the area under the spectrum curve to calculate the inertial cavitation dose (ICD) [28]. The calculation was as follows: the FFT method converted the time-domain signals received into spectra. The spectral area under the bandwidth of the receiving transducer was integrated, and the harmonic from the center frequency of the transmitting HIFU transducer was subtracted to calculate the ICD. This dose was used to describe the threshold for bubble formation.

Additionally, time–frequency signals were plotted to identify the time points at which inertial cavitation occurred. The particle size

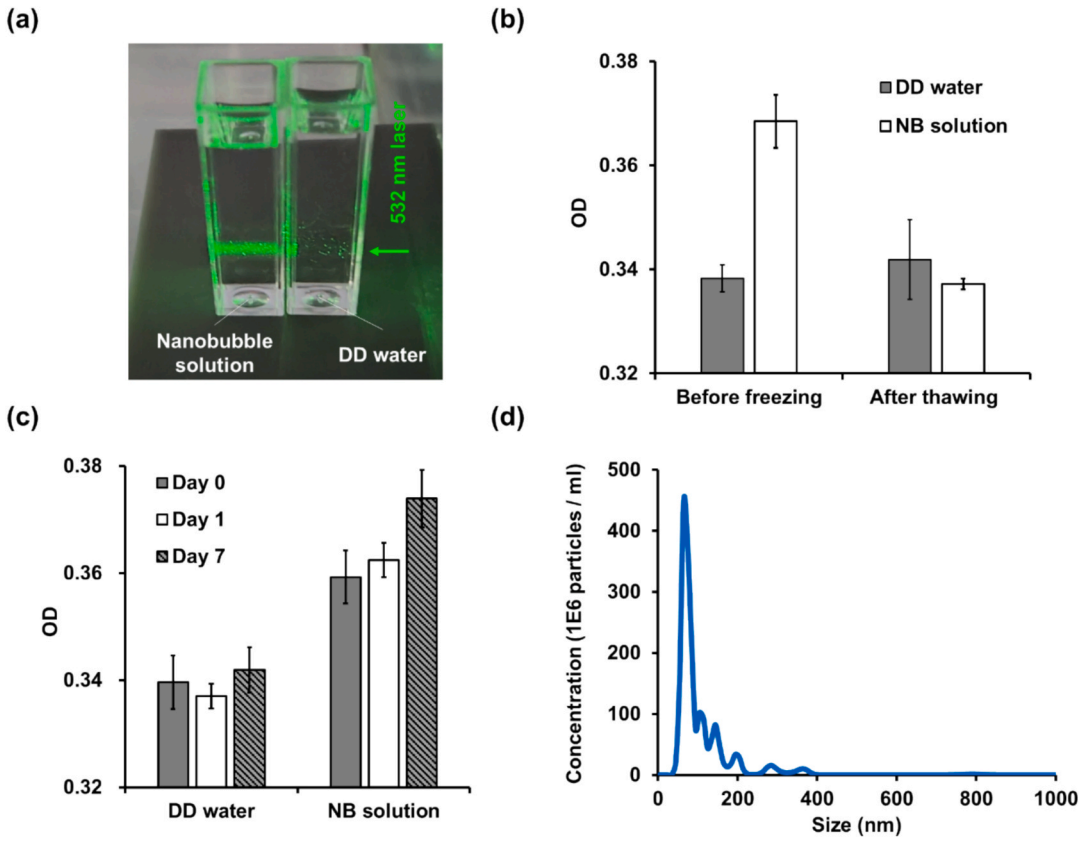

Fig. 2. (a) The laser scattering effect of the nanobubble solution compared with DD water. (b) The freezing and thawing method was used to check the existence of the nanobubbles. (c) The lifetime measurement of the nanobubble solution. (d) The size distribution of the nanobubbles was measured by NanoSight on day 0 after the nanobubbles were generated.

Table 1
NanoSight and DLS measurements of the nanobubble solution on Day 0, Day 1, and Day 7 after generation.

Nanobubble solution state			
	Day 0	Day 1	Day 7
Mean (nm)	107 ± 3.3	110.7 ± 13.8	125.6 ± 1.6
Mode (nm)	73.1 ± 2.8	36.3 ± 19.3	76.6 ± 0.5
D10 (nm)	53.1 ± 1.5	30.7 ± 16.7	71.4 ± 1.3
D50 (nm)	79.5 ± 3.1	79.1 ± 19.6	100.7 ± 5.0
D90 (nm)	166.5 ± 5.8	209.7 ± 21.3	214.4 ± 9.6
Span	1.43	2.26	1.42
Concentration (particles/ml)	$1.94\times10^{9} \pm 1.13 \times 10^{8}$	$1.19\times10^{9} \pm 1.25 \times 10^{8}$	$1.95\times10^{9} \pm 0.98 \times 10^{8}$
Zeta potential (mV)	−21.2 ± 6.84	−29.5 ± 7.74	−27.5 ± 7.76

distribution and zeta potential were measured after 100 cycles of 50-pulse ultrasound exposure at 10.3, 21.2, and 32 MPa, respectively. A total of 2 mL of waste liquid was collected after ultrasound treatment, with 1 mL used for NanoSight analysis and 1 mL for DLS.

3. Results

3.1. Basic properties of nanobubbles

The basic properties of nanobubbles are presented in Fig. 2 and Table 1. As shown in Fig. 2(a), when a laser beam passes through sample bottles containing DD water and an NB solution, a visible trajectory appears only in the NB solution, indicating the presence of nanoparticles. Next, Fig. 2(b) shows that before freezing, the OD values of DD water and the NB solution differ significantly (0.338 ± 0.002 vs. 0.368 ± 0.005). However, after thawing, the OD values become similar (0.342 ± 0.008 vs. 0.337 ± 0.001), suggesting that the nanoparticles were successfully removed during the freezing and thawing process. Based on previous studies, these particles can be identified as nanobubbles [25]. Additionally, Fig. 2(c) demonstrates that the OD values of the NB solution remain stable over 0, 1, and 7 days after generation, indicating that nanobubbles can persist for at least one week. Finally, the size distributions of the nanobubbles measured by NanoSight and DLS were shown in Fig. 2(d). The measurement results on Day 0, Day 1, and Day 7 after generation shown in Table 1 indicated that the average diameter of the nanobubbles is 107 ± 3.3 nm, 110.7 ± 13.8 nm, and 125.6 ± 1.6 nm, respectively. Using the measured D10, D50, and D90 values (representing the sizes below which 10 %, 50 %, and 90 % of the particles fall), the span can be calculated as 1.43, 2.26, and 1.46 (span = (D90-D10)/D50), respectively. A span closer to 0 indicates a more uniform particle size distribution. Additionally, the concentrations of nanobubbles are $1.94 \times 10^{9} \pm 1.13 \times 10^{8}$, $1.19 \times 10^{9} \pm 1.25 \times 10^{8}$, and $1.95 \times 10^{9} \pm 0.98 \times 10^{8}$ particles per mL, with zeta potentials of −21.2 ± 6.84, −29.5 ± 7.74, and −27.5 ± 7.76 mV, respectively.

3.2. Acoustic properties of nanobubbles

High-speed optical images (Fig. 3(a)) show that both DD water and NB solution begin to produce bubbles (visible as black regions in the images) due to the inertial cavitation effect at acoustic pressures above 5.3 MPa. As the acoustic pressure increased, more bubbles were generated. Additionally, at pressures above 5.3 MPa, the NB solution produces more bubbles than the DD water group. Next, Fig. 3(b), (c), (d), and (e) respectively present the time-domain signals, frequency-domain signals, time–frequency signals, and ICD (inertial cavitation dose) values of DD

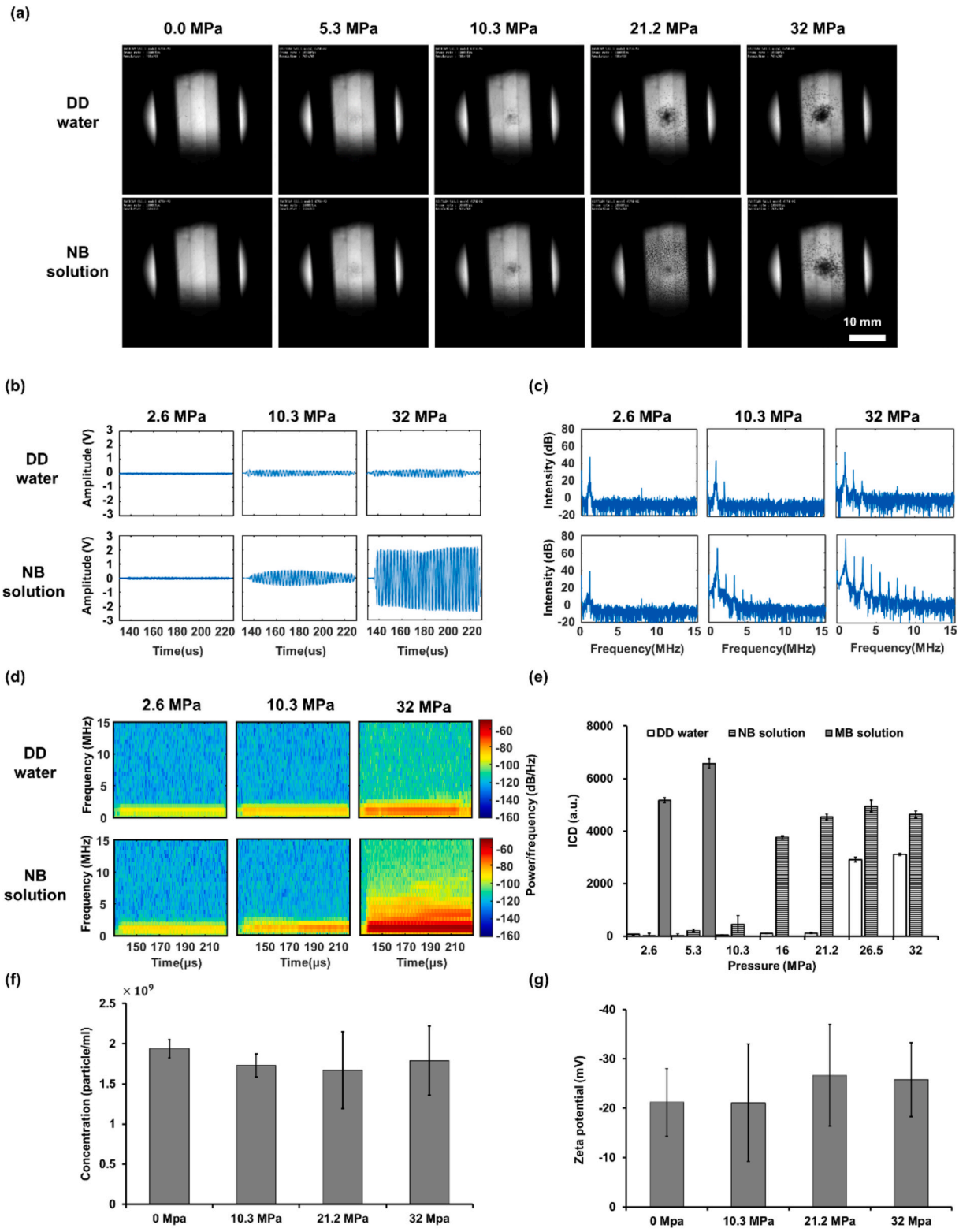

Fig. 3. (a) The high-speed camera image of DD water and NB solution during different pressure exposure. (b) The time domain signal of DD water and NB solution. (c) The frequency spectrum of DD water and NB solution (d) The time–frequency analysis of DD water and NB solution. (e) The ICD calculation of DD water, NB solution comparing with lipid shell microbubble. (f) The concentrations of NB after different ultrasound pressure exposures. (g) The zeta potentials of NB after different ultrasound pressure exposures.

water and NB solution under ultrasonic excitation. The time-domain signals in Fig. 3(b) show that the NB solution receives stronger scattering signals than the DD water group, likely due to the nanobubbles scattering the ultrasound waves. Subsequently, the results in Fig. 3(c) and (d) reveal that the NB solution exhibits earlier and stronger spectral elevation than DD water. This is potentially because the presence of nanobubbles increases the dissolved gas content in water [11], leading to a higher occurrence of inertial cavitation due to the more significant

Table 2
The nanobubbles measurements by NanoSight and DLS after different ultrasound pressure exposures.

Nanobubble solution state				
	0 MPa	10 MPa	21 MPa	32 MPa
Mean (nm)	107 ± 3.3	112.4 ± 9.9	93.1 ± 5.8	134.9 ± 9.9
Mode (nm)	73.1 ± 2.8	68.8 ± 7.3	56.2 ± 5.3	68.8 ± 2.6
D10 (nm)	53.1 ± 1.5	62.8 ± 6.0	49.4 ± 4.0	64.2 ± 1.2
D50 (nm)	79.5 ± 3.1	81.7 ± 6.7	70.7 ± 7.2	115.3 ± 16.1
D90 (nm)	166.5 ± 5.8	185.1 ± 22.7	163.7 ± 11.6	230.2 ± 19.1
Span	1.43	1.50	1.62	1.44
Concentration (particles/ml)	$1.94\times10^{9} \pm 1.13 \times 10^{8}$	$1.73\times10^{9} \pm 1.43 \times 10^{8}$	$1.67 \times 10^{9} \pm 4.77 \times 10^{8}$	$1.79 \times 10^{9} \pm 4.31 \times 10^{8}$
Zeta potential (mV)	−21.2 ± 6.84	−21.1 ± 11.9	−26.7 ± 10.3	−25.8 ± 7.5

number of gas nuclei. Finally, Fig. 3(e) compares the ICD values of DD water and the nanobubble solution while also including MB, a conventional ultrasound contrast agent (The detail of the microbubble results was shown in Fig. S1. in the support information) as a control. The results indicate that MB produces inertial cavitation effects at pressures as low as 2.6 MPa. In DD water, the acoustic pressure required for inertial cavitation is approximately 26.5 MPa. However, in the presence of nanobubbles, the acoustic pressure threshold for inertial cavitation decreases to 10.3 MPa, which indicates the interaction between nanobubbles and high-pressure ultrasound. The nanobubbles concentration, size distribution, and zeta potential results, shown in Fig. 3(f)(g) and Table 2, indicate no significant difference before and after ultrasound treatment, suggesting that the nanobubbles were not collapsed by ultrasound.

4. Discussion

This study confirms that the claw-type pump can generate nanobubble solutions with the nanobubbles ranging from 53.1 to 166.5 nm with a concentration of 1.9 billion particles per ml, which is smaller than the values reported in the literature [22]. These nanobubbles exhibit a uniform size distribution (span = 1.43), high particle stability (lifetime > 1 week), and a negative surface potential (zeta potential = -21.2 mV). Unlike the acoustic cavitation method mentioned in the literature [23], which controls nanobubbles concentration by adjusting the ultrasound frequency, the claw-type pump method allows for concentration control by tuning the rotation speed of the motor and the design of the claw-shaped rotors.

The acoustic experimental results showed that the spectral elevation signals generated by the nanobubble solution under high acoustic pressure were similar to those of DD water but different from those of MBs. The nanobubbles concentration and zeta potential results indicate no significant difference before and after ultrasound treatment, suggesting that nanobubbles were likely not ruptured by ultrasound but instead acted as speckles in the solution. Compared to other research, the reason our nanobubbles did not collapse during ultrasound exposure may be due to differences in the generation method and ultrasound frequency of 1.1 MHz in our research, compared to the wideband shock wave [29] and 5 MHz frequency transducer [30] used in the literature. This hypothesis is further supported by the presence of abundant harmonic signals in the 32 MPa NB solution group. Additionally, the inertial cavitation threshold of the NB solution was lower compared to DD water (10.3 MPa vs 26.5 MPa). This may be attributed to the increased number of gas nuclei in the NB solution [12], making the solution more prone to inertial cavitation effects and generating many bubbles (Fig. 3(a)). Furthermore, our spectrum results are similar to the passively received signals during histotripsy in the previous study that used the same ultrasound parameters [31]. As a result, these findings may provide a potential approach to enhance the treatment efficiency of ultrasound histotripsy.

Based on the current results, we have successfully characterized the basic properties and acoustic features of these nanobubbles. Future research will investigate advanced characteristics, such as surface functional groups and the gas composition within the bubbles. These properties will help uncover the mechanisms of nanobubble interactions and facilitate their applications in areas such as wastewater purification, aquaculture, agriculture, and industrial processes.

Declaration of Generative AI and AI-assisted technologies in the writing process:

During the preparation of this work the author(s) used Chat-GPT in order to improve language and readability. After using this tool, the author(s) reviewed and edited the content as needed and take(s) full responsibility for the content of the publication.

Data and materials availability

All data needed to evaluate the conclusions in the paper are provided within the paper and/or the Supplementary Materials and are available from the corresponding author upon request.

CRediT authorship contribution statement

Zong-Han Hsieh: Writing – review & editing, Writing – original draft, Visualization, Validation, Methodology, Data curation. **Cheng-An J. Lin:** Supervision, Resources, Formal analysis, Data curation. **Chih-Kuang Yeh:** Writing – review & editing, Validation, Supervision, Project administration, Funding acquisition, Formal analysis, Conceptualization.

Funding

The authors gratefully acknowledge the support of the National Science and Technology Council, Taiwan, under Grant Nos. 111-2221-E-007-019-MY3, 113-2221-E-007-022-MY3.

Declaration of competing interest

The authors declare that they have no known competing financial interests or personal relationships that could have appeared to influence the work reported in this paper.

Appendix A. Supplementary data

Supplementary data to this article can be found online at https://doi.org/10.1016/j.ultsonch.2025.107336.

References

[1] Z. Xu, T.D. Khokhlova, C.S. Cho, V.A. Khokhlova, Histotripsy: A Method for Mechanical Tissue Ablation with Ultrasound, (2025). doi: 10.1146/annurev-bioeng-073123.

[2] Z. Xu, T.L. Hall, E. Vlaisavljevich, F.T. Lee, Histotripsy: the first noninvasive, non-ionizing, non-thermal ablation technique based on ultrasound, Int. J. Hyperth. 38 (2021) 561–575, https://doi.org/10.1080/02656736.2021.1905189.
[3] Y.S. Tung, J.J. Choi, B. Baseri, E.E. Konofagou, Identifying the inertial cavitation threshold and skull effects in a vessel phantom using focused ultrasound and microbubbles, Ultrasound Med. Biol. 36 (2010) 840–852, https://doi.org/10.1016/j.ultrasmedbio.2010.02.009.
[4] T. Yin, P. Wang, R. Zheng, B. Zheng, D. Cheng, X. Zhang, X. Shuai, Nanobubbles for enhanced ultrasound imaging of tumors, Int. J. Nanomed. 7 (2012) 895–904, https://doi.org/10.2147/IJN.S28830.
[5] Z. Xing, J. Wang, H. Ke, B. Zhao, X. Yue, Z. Dai, J. Liu, The fabrication of novel nanobubble ultrasound contrast agent for potential tumor imaging, Nanotechnology 21 (2010), https://doi.org/10.1088/0957-4484/21/14/145607.
[6] D.V.B. Batchelor, F.J. Armistead, N. Ingram, S.A. Peyman, J.R. McLaughlan, P. L. Coletta, S.D. Evans, The influence of nanobubble size and stability on ultrasound enhanced drug delivery, Langmuir 38 (2022) 13943–13954, https://doi.org/10.1021/acs.langmuir.2c02303.
[7] D.V.B. Batchelor, R.H. Abou-Saleh, P.L. Coletta, J.R. McLaughlan, S.A. Peyman, S. D. Evans, Nested nanobubbles for ultrasound-triggered drug release, ACS Appl. Mater. Interfaces 12 (2020) 29085–29093, https://doi.org/10.1021/acsami.0c07022.
[8] E. Bakalis, P. Efthymiopoulos, F. Lugli, A.C. Mitropoulos, G.Z. Kyzas, F. Zerbetto, Nanobubbles in ultrapure water can self-propel, ChemPhysChem (2024), https://doi.org/10.1002/cphc.202400508.
[9] K. Ohgaki, N.Q. Khanh, Y. Joden, A. Tsuji, T. Nakagawa, Physicochemical approach to nanobubble solutions, Chem. Eng. Sci. 65 (2010) 1296–1300, https://doi.org/10.1016/j.ces.2009.10.003.
[10] J.N. Meegoda, S. Aluthgun Hewage, J.H. Batagoda, Stability of nanobubbles, Environ, Eng. Sci. 35 (2018) 1216–1227, https://doi.org/10.1089/ees.2018.0203.
[11] A. Tekile, I. Kim, J.Y. Lee, Extent and persistence of dissolved oxygen enhancement using nanobubbles, Environ. Eng. Res. 21 (2016) 427–435, https://doi.org/10.4491/eer.2016.028.
[12] A.J. Atkinson, O.G. Apul, O. Schneider, S. Garcia-Segura, P. Westerhoff, Nanobubble technologies offer opportunities to improve water treatment, Acc. Chem. Res. 52 (2019) 1196–1205, https://doi.org/10.1021/acs.accounts.8b00606.
[13] K. Yasui, T. Tuziuti, N. Izu, W. Kanematsu, Is surface tension reduced by nanobubbles (ultrafine bubbles) generated by cavitation? Ultrason. Sonochem. 52 (2019) 13–18, https://doi.org/10.1016/j.ultsonch.2018.11.020.
[14] X. Bu, S. Zhou, X. Tian, C. Ni, S. Nazari, M. Alheshibri, Effect of aging time, airflow rate, and nonionic surfactants on the surface tension of bulk nanobubbles water, J. Mol. Liq. 359 (2022), https://doi.org/10.1016/j.molliq.2022.119274.
[15] A. Ushida, T. Hasegawa, N. Takahashi, T. Nakajima, S. Murao, T. Narumi, H. Uchiyama, Effect of mixed nanobubble and microbubble liquids on the washing rate of cloth in an alternating flow, J. Surfactant Deterg. 15 (2012) 695–702, https://doi.org/10.1007/s11743-012-1348-x.
[16] S. Zhou, S. Nazari, A. Hassanzadeh, X. Bu, C. Ni, Y. Peng, G. Xie, Y. He, The effect of preparation time and aeration rate on the properties of bulk micro-nanobubble water using hydrodynamic cavitation, Ultrason. Sonochem. 84 (2022), https://doi.org/10.1016/j.ultsonch.2022.105965.
[17] S. Zhou, W. Zhou, L. Dong, Y. Peng, G. Xie, Micellization Transformations of Sodium Oleate Induced by Gas Nucleation, Langmuir 37 (2021) 9701–9710, https://doi.org/10.1021/acs.langmuir.1c01008.
[18] M.U. Farid, P.J. Choi, J.A. Kharraz, J.Y. Lao, S. St-Hilaire, Y. Ruan, P.K.S. Lam, A. K. An, Hybrid nanobubble-forward osmosis system for aquaculture wastewater treatment and reuse, Chem. Eng. J. 435 (2022), https://doi.org/10.1016/j.cej.2022.135164.
[19] S. Yaparatne, J. Morón-López, D. Bouchard, S. Garcia-Segura, O.G. Apul, Nanobubble applications in aquaculture industry for improving harvest yield, wastewater treatment, and disease control, Sci. Total Environ. 931 (2024), https://doi.org/10.1016/j.scitotenv.2024.172687.
[20] A. Agarwal, W.J. Ng, Y. Liu, Principle and applications of microbubble and nanobubble technology for water treatment, Chemosphere 84 (2011) 1175–1180, https://doi.org/10.1016/j.chemosphere.2011.05.054.
[21] S. Liu, S. Oshita, S. Kawabata, Y. Makino, T. Yoshimoto, Identification of ROS produced by nanobubbles and their positive and negative effects on vegetable seed germination, Langmuir 32 (2016) 11295–11302, https://doi.org/10.1021/acs.langmuir.6b01621.
[22] X. Bu, M. Alheshibri, The effect of ultrasound on bulk and surface nanobubbles: A review of the current status, Ultrason. Sonochem. 76 (2021), https://doi.org/10.1016/j.ultsonch.2021.105629.
[23] K. Yasuda, H. Matsushima, Y. Asakura, Generation and reduction of bulk nanobubbles by ultrasonic irradiation, Chem. Eng. Sci. 195 (2019) 455–461, https://doi.org/10.1016/j.ces.2018.09.044.
[24] Tien-Tung, Chung, Lin Heng, Chuang Feng-Ming, Double-lobe type rotor design process, U.S. Patent No.7.255,545, 2007.
[25] N. Nirmalkar, A.W. Pacek, M. Barigou, On the existence and stability of bulk nanobubbles, Langmuir 34 (2018) 10964–10973, https://doi.org/10.1021/acs.langmuir.8b01163.
[26] S.T. Kang, C.K. Yeh, Ultrasound microbubble contrast agents for diagnostic and therapeutic applications: Current status and future design, Chang Gung Med. J. 35 (2012) 125–139, https://doi.org/10.4103/2319-4170.106159.
[27] K.B. Bader, E. Vlaisavljevich, A.D. Maxwell, For whom the bubble grows: physical principles of bubble nucleation and dynamics in histotripsy ultrasound therapy, Ultrasound Med. Biol. 45 (2019) 1056–1080, https://doi.org/10.1016/j.ultrasmedbio.2018.10.035.
[28] W.S. Chen, A.A. Brayman, T.J. Matula, L.A. Crum, Inertial cavitation dose and hemolysis produced in vitro with or without Optison®, Ultrasound Med. Biol. 29 (2003) 725–737, https://doi.org/10.1016/S0301-5629(03)00013-9.
[29] J.M. Rosselló, C.D. Ohl, Clean production and characterization of nanobubbles using laser energy deposition, Ultrason. Sonochem. 94 (2023), https://doi.org/10.1016/j.ultsonch.2023.106321.
[30] J.M. Rosselló, C.D. Ohl, On-demand bulk nanobubble generation through pulsed laser illumination, PhysRevLett 127 (2021), https://doi.org/10.1103/PhysRevLett.127.044502.
[31] K.J. Pahk, D.K. Dhar, M. Malago, N. Saffari, Ultrasonic histotripsy for tissue therapy, J. Phys. Conf. Ser., Inst. Phys. Publ. (2015), https://doi.org/10.1088/1742-6596/581/1/012001.